Zhaobo Qin
Department of Automobile Engineering,
Tsinghua University,
Beijing 100084, China;
Department of Mechanical Engineering,
University of Michigan,
Ann Arbor, MI 48105
e-mail: qzb13@mails.tsinghua.edu.cn

Yugong Luo
Department of Automobile Engineering,
Tsinghua University,
Beijing 100084, China
e-mail: lyg@tsinghua.edu.cn

Keqiang Li[1]
Department of Automobile Engineering,
Tsinghua University,
Beijing 100084, China
e-mail: likq@tsinghua.edu.cn

Huei Peng
Fellow ASME
Department of Mechanical Engineering,
University of Michigan,
Ann Arbor, MI 48105
e-mail: hpeng@umich.edu

Optimal Design of Single-Mode Power-Split Hybrid Tracked Vehicles

Hybrid tracked vehicles are common in construction, agriculture, and military applications. Most use a series hybrid powertrain with large motors and operate at a relatively low efficiency. Although some researchers have proposed power-split powertrains, most of these would require an additional mechanism to achieve skid steering. To solve this problem and enhance drivability, a single-mode power-split hybrid powertrain for tracked vehicles with two outputs connected to the left and right tracks is proposed. The powertrain with three planetary gears (PGs) would then be able to control the torque on the two tracks independently and achieve skid steering. This powertrain has three degrees-of-freedom (DOF), allowing for control of the output torques and the engine speed independently from the vehicle running speed. All design candidates with three PGs are exhaustively searched by analyzing the dynamic characteristics and control to obtain the optimal design. Efficient topology design selection with parameter sizing and component sizing is accomplished using the enhanced progressive iteration approach to achieve better fuel economy using downsized components. [DOI: 10.1115/1.4039687]

Keywords: track-type dozer, optimal control, planetary gear, optimal design

1 Introduction

Ever since Toyota released the Prius as first generation of power-split hybrid cars at the end of last century, power-split vehicles have continued to dominate the hybrid vehicle market. Since the introduction of the Toyota hybrid system [1], many other power-split designs have also been proposed [2,3]. In the U.S., more than 80% of all hybrid vehicles sold in 2016 were power-split types [4], which utilized planetary gears (PGs) as the transmission device. Powertrains using planetary gears can realize a continuously variable transmission function with high torque capacity and a compact size [5]. Power-split hybrid powertrains are widely designed and analyzed using the lever diagram [6]. A methodology for exhaustive search of power-split hybrid designs has been proposed by establishing automated dynamics modeling with two planetary gears [7]. Power-split hybrids are classified into input-split, output-split, and compound split types [8] with different characteristics [9]. To further improve the vehicle performance, multimode power-split designs have been studied [10]. Different operating modes were achieved through the control of clutches. To systematically explore all possible multimode designs for passenger cars, a design approach was presented that enabled a fast and exhaustive search with various clutch location [11]. Graph theory could also be applied to investigate the design topologies automatically [12,13]. In addition to passenger cars, light or heavy duty trucks can also use power-split hybrids. Optimal designs for hydraulic trucks have been studied, which can achieve superior fuel economy [14]. Recently, an innovative four-wheel drive power split design for light trucks has been presented, where the powertrain device has two output shafts connected to the two drive axles [15].

Most power-split hybrids are applied to wheeled vehicles, while few hybrid tracked vehicles deployed power-split powertrains. Most tracked vehicles focus on series hybrid designs instead. In 2002, Caterpillar released their first series hybrid track type dozer (TTD) called D7E, which reduces fuel consumption by 20% compared with the traditional diesel-powered design. D7E has been commercialized and is enjoying healthy sales [16]. Researches are also being conducted about hybrid tracked vehicles. A dual-motor series hybrid powertrain was proposed that can be used for heavy duty tracked vehicles [17]. However, as the power necessary to achieve skid-steering can be much larger than that needed during straight driving [18], large motors must be used or an additional steering mechanism is required [19]—a significant disadvantage of such hybrid tracked vehicles. Power-split hybrid tracked vehicles have rarely been studied because of their complex structure. A dual-mode compound split powertrain for tracked vehicles has been invented, which has an additional steering mechanism powered by another steering motor [20]. Power-split hybrids can not only have better fuel economy and performance compared with the series hybrid designs, but also be designed to have two output shafts for the left and right tracks of tracked vehicles, achieving skid steering without extra steering mechanisms. However, the design methodologies for power-split tracked vehicles remain unexplored.

The optimal design of power-split hybrids is a multilayer optimization problem that involves not only topology but also size [21]. Many of the aforementioned studies have explored the topology search space but have not searched the space of sizing. Sizing parameters for hybrid vehicles can be dealt with in many ways. A genetic algorithm-based methodology has been used for parameter sizing of hybrid vehicles [22]. Evolutionary algorithms were widely used to conduct a multi-objective parameter optimization [23]. Many other heuristic algorithms such as bees-algorithm and PSO-algorithm have been applied [24,25]. These studies focused on parameter sizing but did not cover topology variation. An optimal sizing method was proposed with a hierarchical optimization process for heavy hybrid electric trucks. When the sizing pool is

[1]Corresponding author.

Contributed by the Dynamic Systems Division of ASME for publication in the Journal of Dynamic Systems, Measurement, and Control. Manuscript received April 24, 2017; final manuscript received March 14, 2018; published online May 2, 2018. Assoc. Editor: Ardalan Vahidi.

large, however, the convergence rate is slow [17]. A simultaneous optimization of topology and sizing was then presented using iterative optimization which can quickly determine the gear ratios and topology. However, the sizes of power elements are not considered [26].

By integrating multiple levels (topology, size, and control), we focus on the design of a power-split hybrid TTD in this paper. The left and right tracks must be controlled independently to be able to drive straight and achieve skid steering. In addition, the engine should always operate efficiently to achieve superior fuel economy, which means that powertrains need to have three degrees-of-freedom (DOF), one more than the power-split passenger cars [7]. Moreover, parameter sizing, topology screening, and optimal control are all executed to ensure optimal performance. The contributions of this paper are summarized below:

(1) A novel hybrid propulsion system is proposed, which uses the powertrain with three PGs. The design uses one engine and three electric motors, and can be used as the promising powertrain of TTDs with two output shafts to control the left and right tracks separately. The design achieves skid-steering without the use of a steering mechanism. It improves both driving performance and fuel economy.
(2) A novel systematic methodology is presented by searching through both the topology and the parameter sizing design space using a progressive iteration approach together with the optimal control. The sizing parameters including the ratios of the three planetary gears, the final drives of the two outputs, and the size of the engine, three motors and the battery. Instead of a brute-force search, a progressive rule is used for each iteration, which is computationally more efficient. The methodology can be applied to identify the optimal design of a complex multiple PG system rapidly.

The remainder of the paper is organized as follows: In Sec. 2, we describe the design approach and the design objectives of the hybrid power-split TTD. Section 3 describes the automated modeling of the powertrain dynamics. In Sec. 4, we discuss the rapid screening technique, which identifies the optimal design that satisfies all the requirements. In Sec. 5, parameter sizing is searched to find the optimal design. Finally, conclusions are drawn in Sec. 6.

2 Objective and Procedure

The design consists of three motors, two outputs, and an engine as stated previously in Sec. 1. Therefore, in this paper, design using three PGs, with a third motor to control 3DOF, is studied. To evaluate the benefits of the proposed design, a series hybrid TTD is used as the benchmark [27]. The series hybrid TTD has one engine, one generator, and two motors connected to both sides of tracks. The schematic diagram of the series benchmark is shown in Fig. 1 and the key parameters of the benchmark vehicle are given in Table 1.

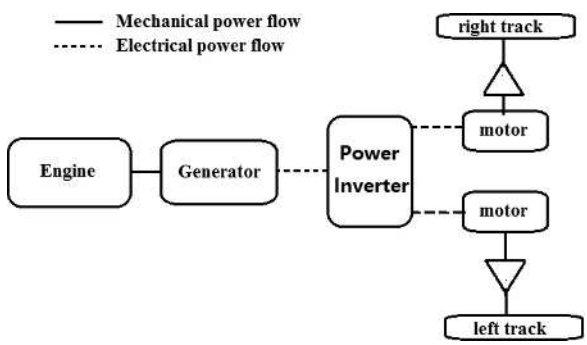

Fig. 1 Schematic diagram of the benchmark series hybrid TTD

There are three nodes in each PG, namely, the sun gear, the carrier gear, and the ring gear. Since there can be a number of possible connections among PG nodes and components, a design generation method is given in Fig. 2 by using a lever diagram, with MG representing the motor. R, C, and S are the ring, carrier, and sun gears of the PG. When components are connected with nodes in PGs, configuration is generated; when the connections are determined, a design is generated. If the framework includes two PGs and six components, there can be only $P_6^6 = 720$ configurations and $P_6^6 C_{16}^1 = 1.15 \times 10^4$ design candidates [11]. The design flexibility will be limited. Furthermore, since the traction torque of TTDs can be large, three PGs can have much towing capacity than two PGs [28]. Thus, three PGs are selected to provide a large design space and meet the towing requirements.

Since there are 2DOF for each PG, three PGs have 6DOF to start. To obtain a 3DOF design, three constraints are imposed (through node connections). How and where to add the constraints is a major decision in the design process. The overall design procedure is presented in Fig. 3.

First, all feasible designs are modeled using the automated modeling method. Since many designs do not have the desired attributes or performance, an efficient and rapid screening method must be used. The screening process consists of four steps. The first step ensures that two outputs can be controlled independently and that the vehicle can drive backward by motors. The maximum towing capacity is checked in the second step. The maximum traction torque and the minimum turning radius are checked in the third step. In the fourth step, fuel economy under straight driving and turning are computed using the dynamic programming (DP) technique. Finally, for the superior designs identified, an enhanced progressive iteration method is used to search both topology designs and sizing parameters to obtain the final optimal design.

3 Automated Dynamics Modeling

The dynamics of tracked vehicles differ from those of the wheeled vehicles. Not only straight driving but also skid steering must be taken into account. The straight driving pulling force can be calculated in Eq. (1). There are two kinds of longitudinal force: driving resistance F_D and bulldozing resistance F_B. Driving resistance consists of air resistance, rolling resistance, and grade resistance

$$\begin{aligned} F_f &= F_D + F_B \\ F_D &= C_D A \left(\frac{v}{3.6}\right)^2 + G\sin\alpha + Gf\cos\alpha \\ F_B &= k_b B_c h + \frac{\rho\mu_1 B_c (H-h)^2}{2k_m \tan\phi} + k_y B_c x \mu_2 + G\mu_2 \cos^2\delta \end{aligned} \tag{1}$$

Table 1 Key parameters of the benchmark TTD

	Parameter	Value
Vehicle	Vehicle mass with rated load (kg)	28,000
	Track length (m)	2.73
	Track gauge (m)	1.786
Engine	Engine displacement (L)	9.3
	Rated speed (rpm)	1700
	Rated power (kW)	200
Generator	Max. power (kW)	180
	Max. rotational speed (rpm)	2400
Motors	Rated power (kW)	85
	Max. rotational speed (rpm)	6200
Battery	Capacity (Ah)	45

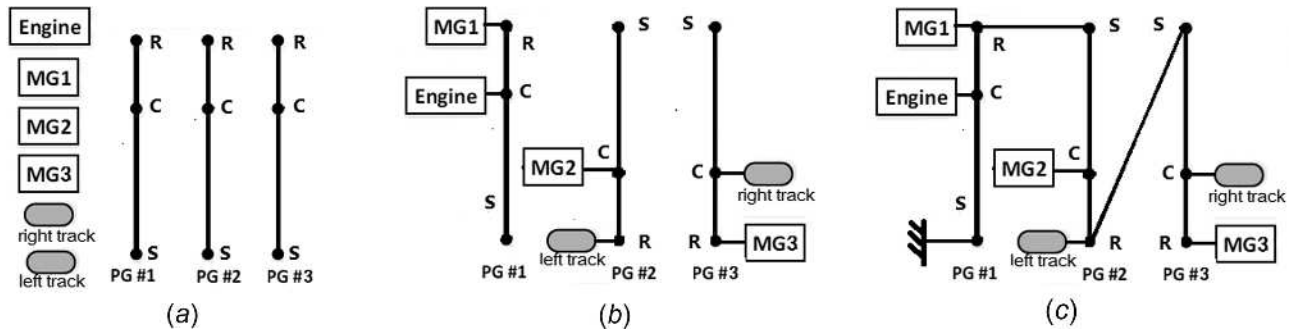

Fig. 2 Framework, configuration, and design generation

where C_D is the air resistance coefficient, A is the windward area, v is the velocity, G is the running weight, f is the rolling resistance coefficient, α is the gradient, k_b is the cutting force per unit area, B_c and h are the breadth and the cutting depth of dozer blade, respectively, H is the blade height, ρ is the soil density, μ_1 and μ_2 are the rolling resistance of soil–soil and soil–steel, respectively, k_m is the soil filling coefficient, ϕ is the soil angle of gradient, k_y and x are the specific resistance and contact area between soil and cutting edge, respectively, and δ is the cutting angle of moldboard. The final longitudinal force will be distributed to the two sides of the track evenly (details can be seen in Ref. [29]).

For skid steering, with turning radius R, the turning force on each side of the tracks can be explained as follows:

$$\begin{aligned} F_2 + F_1 - F_f &= m\dot{v}_c \\ (F_2 - F_1)\frac{B}{2} - \frac{\mu G L}{4} - (F_{g2} - F_{g1})\frac{B}{2} &= \dot{\omega}_c I \end{aligned} \tag{2}$$

$$\mu = \frac{\mu_{\max}}{\left(0.925 + 0.15\dfrac{B}{R}\right)} \tag{3}$$

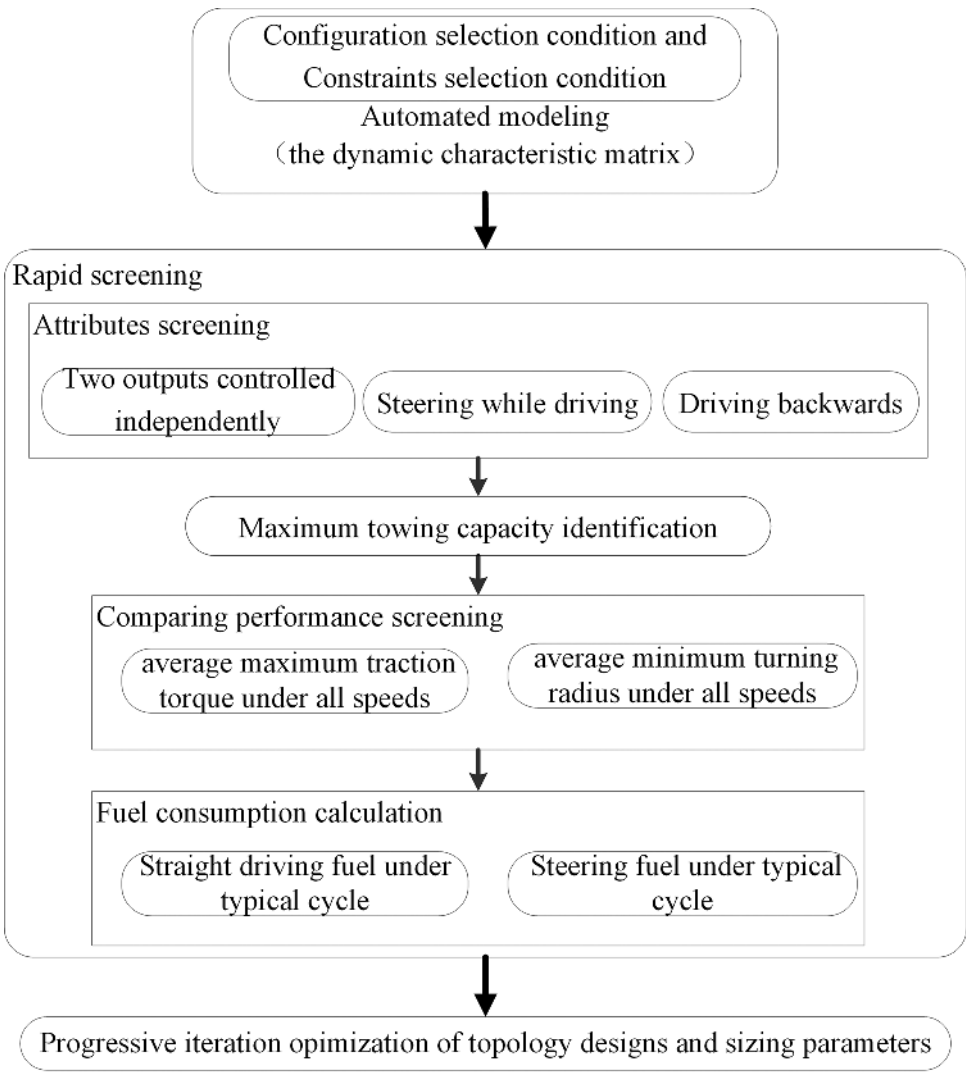

Fig. 3 The overall design procedure

$$\begin{cases} F_1 = -\dfrac{F_f + ma_c}{2} + \dfrac{G\mu L}{4B} + \dfrac{I}{B}\dot{\omega}_c \\ F_2 = -\dfrac{F_f + ma_c}{2} - \dfrac{G\mu L}{4B} - \dfrac{I}{B}\dot{\omega}_c \end{cases} \tag{4}$$

where F_f equals the total longitudinal force, F_{g1} and F_{g2} are the transverse force, v_c, ω_c, and a_c are the speed, rotation speed, and acceleration of central barycenter, respectively, m is the vehicle mass, I is the inertial of the vehicle, B is the width between two tracks, and $\mu_{\max}$ is the turning resistance coefficient of certain soil. Since the transverse force on each track differs little, F_{g2} and F_{g1} are approximately equal.

Given the vehicle dynamics and the basic design structure in Fig. 2, all 3DOF designs are exhaustively searched. First, we assign the components to the nine nodes of 3PGs, which result in many different configurations, each with a specific connection between the components and the PGs. There are $P_9^6 = 60,480$ different configurations. Then, three constraints are added using permanent connections between two nodes or brakes to ground a node. There are $C_9^2 + C_9^1 = 45$ different permanent connections shown in Fig. 4. The solid lines indicate the linking connections of two nodes and grounding connections, respectively.

Some of the connections are redundant, indicated by dashed lines in Fig. 4. In a single PG, connecting any two nodes results in equivalent designs because all three nodes will rotate at the same speed. In addition, the output shafts should not be grounded, which means that there are $45 - 2 \times 3 - 2 = 37$ legitimate connections.

To identify all feasible designs, an automated modeling method is used to obtain the governing equation. Take the design in Fig. 5 as an example.

An analysis of the dynamics of all nodes in Fig. 5(*a*) independently yields the following equation:

$$\left[\begin{array}{ccccccccc|ccc}
I_e+I_{r2} & 0 & 0 & 0 & 0 & 0 & 0 & 0 & 0 & 0 & -R_2 & 0 \\
0 & I_{v_l}+I_{c1} & 0 & 0 & 0 & 0 & 0 & 0 & 0 & R_1+S_1 & 0 & 0 \\
0 & 0 & I_{v_r}+I_{c3} & 0 & 0 & 0 & 0 & 0 & 0 & 0 & 0 & R_3+S_3 \\
0 & 0 & 0 & I_{\mathrm{mg1}}+I_{r2} & 0 & 0 & 0 & 0 & 0 & 0 & R_2+S_2 & 0 \\
0 & 0 & 0 & 0 & I_{\mathrm{mg2}}+I_{r1} & 0 & 0 & 0 & 0 & -R_1 & 0 & 0 \\
0 & 0 & 0 & 0 & 0 & I_{\mathrm{mg3}}+I_{r3} & 0 & 0 & 0 & 0 & 0 & -R_3 \\
0 & 0 & 0 & 0 & 0 & 0 & I_{s1} & 0 & 0 & -S_1 & 0 & 0 \\
0 & 0 & 0 & 0 & 0 & 0 & 0 & I_{s2} & 0 & 0 & -S_2 & 0 \\
0 & 0 & 0 & 0 & 0 & 0 & 0 & 0 & I_{s3} & 0 & 0 & -S_3 \\
\hline
0 & R_1+S_1 & 0 & 0 & -R_1 & 0 & -S_1 & 0 & 0 & 0 & 0 & 0 \\
-R_2 & 0 & 0 & R_2+S_2 & 0 & 0 & 0 & -S_2 & 0 & 0 & 0 & 0 \\
0 & 0 & R_3+S_3 & 0 & 0 & -R_3 & 0 & 0 & -S_3 & 0 & 0 & 0
\end{array}\right]
\left[\begin{array}{c} \dot{\omega}_e \\ \dot{\omega}_{v_l} \\ \dot{\omega}_{v_r} \\ \dot{\omega}_{\mathrm{mg1}} \\ \dot{\omega}_{\mathrm{mg2}} \\ \dot{\omega}_{\mathrm{mg3}} \\ \dot{\omega}_{\mathrm{sp1}} \\ \dot{\omega}_{\mathrm{sp2}} \\ \dot{\omega}_{\mathrm{sp3}} \\ F_1 \\ F_2 \\ F_3 \end{array}\right]
=
\left[\begin{array}{c} T_e \\ T_{v_l} \\ T_{v_r} \\ T_{\mathrm{mg1}} \\ T_{\mathrm{mg2}} \\ T_{\mathrm{mg3}} \\ 0 \\ 0 \\ 0 \\ 0 \\ 0 \\ 0 \end{array}\right]$$

$$\begin{bmatrix} J & D \\ D^T & 0 \end{bmatrix} \begin{bmatrix} \dot{\Omega} \\ F \end{bmatrix} = \begin{bmatrix} T \\ 0 \end{bmatrix} \tag{5}$$

In Eq. (5), R_i and S_i are, respectively, the radii of the ring gear and sun gear for the ith PG set. I_e, I_{v_l}, I_{v_r}, I_{mg1}, I_{mg2}, and I_{mg3} represent, respectively, the rotational inertia of the engine, left output, right output, and motors. T and $\dot{\omega}$ represent the torque and angular acceleration of the components, respectively. F_1, F_2, and F_3 represent the internal force of the three PG sets.

Equation (5) is governed by the inertia matrix **J**, speed and torque matrices $\dot{\mathbf{\Omega}}$ and **T**, internal force matrix **F**, and the **D** matrix, which corresponds to a unique design. The rules for automatically obtaining the **D** matrix can be found in Ref. [7].

When permanent connections are added, the matrices will change accordingly. A new modeling method is proposed here that can be applied to all PG powertrain designs. Compared with some previous methods, the method proposed here can improve computational efficiency under all circumstances. Define a unit matrix $I_{3n\times 3n}$, where n represents the number of planetary gears, then follow the rules below to manipulate this matrix. If the ath node is connected to the bth node, add the elements of the ath row to the bth row, then remove the ath row. If the ath node is grounded, then remove the ath row. After all constraints are added, the original **I** matrix is transformed into a new matrix **N** with a dimension $(3n - c) \times 3n$, where c is the number of connections. Then, a new matrix can be generated with the following transformation and Eq. (5) also changes:

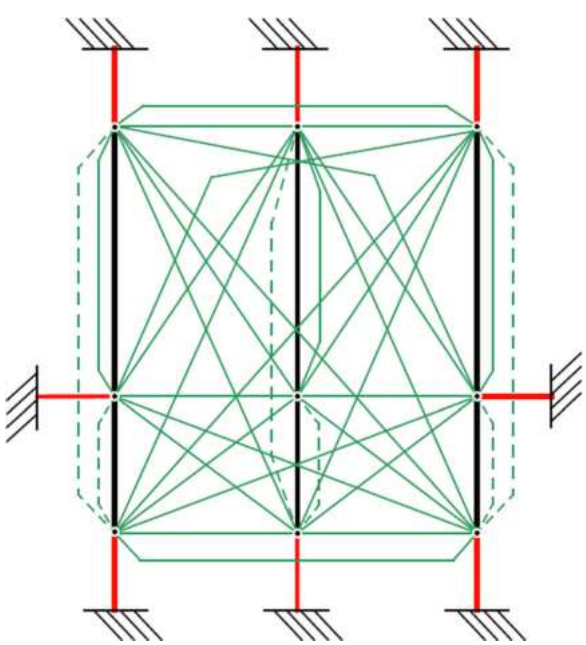

Fig. 4 All possible permanent connections for a configuration

$$D^* = N \cdot D \cdot J^* = NJN^T,\ \Omega^* = N \cdot \Omega, T^* = N \cdot T$$

$$\begin{bmatrix} I_e + I_{r2} & 0 & 0 & 0 & 0 & 0 & 0 & -R_2 & 0 \\ 0 & I_{V\_l} + I_{c1} & 0 & 0 & 0 & 0 & R_1 + S_1 & 0 & 0 \\ 0 & 0 & I_{V\_r} + I_{c3} & 0 & 0 & 0 & 0 & 0 & R_3 + S_3 \\ 0 & 0 & 0 & I_{\mathrm{mg1}} + I_{c2} & 0 & 0 & 0 & R_2 + S_2 & 0 \\ 0 & 0 & 0 & 0 & I_{\mathrm{mg2}} + I_{r1} & 0 & -R_1 & 0 & 0 \\ 0 & 0 & 0 & 0 & 0 & I_{\mathrm{mg3}} + I_{r3} + I_{s1} + I_{s2} & -S_1 & -S_2 & -R_3 \\ 0 & R_1 + S_1 & 0 & 0 & -R_1 & -S_1 & 0 & 0 & 0 \\ -R_2 & 0 & 0 & R_2 + S_2 & 0 & -S_2 & 0 & 0 & 0 \\ 0 & 0 & R_3 + S_3 & 0 & 0 & -R_3 & 0 & 0 & 0 \end{bmatrix} \begin{bmatrix} \dot{\omega}_e \\ \dot{\omega}_{V\_l} \\ \dot{\omega}_{V\_r} \\ \dot{\omega}_{\mathrm{mg1}} \\ \dot{\omega}_{\mathrm{mg2}} \\ \dot{\omega}_{\mathrm{mg3}} \\ F_1 \\ F_2 \\ F_3 \end{bmatrix} = \begin{bmatrix} T_e \\ T_{V\_l} \\ T_{V\_r} \\ T_{\mathrm{mg1}} \\ T_{\mathrm{mg2}} \\ T_{\mathrm{mg3}} \\ 0 \\ 0 \\ 0 \end{bmatrix} \tag{6}$$

The relationships of all torques and speeds terms are then governed by the below equation:

$$\begin{bmatrix} \dot{\omega}_e \\ \dot{\omega}_{V\_l} \\ \dot{\omega}_{V\_r} \\ \dot{\omega}_{\mathrm{mg1}} \\ \dot{\omega}_{\mathrm{mg2}} \\ \dot{\omega}_{\mathrm{mg3}} \end{bmatrix} = \mathbf{A}^* \begin{bmatrix} T_e \\ T_{V\_l} \\ T_{V\_r} \\ T_{\mathrm{mg1}} \\ T_{\mathrm{mg2}} \\ T_{\mathrm{mg3}} \end{bmatrix} \tag{7}$$

The matrix **A*** is obtained through the following derivations.

Assume that

$$\begin{bmatrix} \mathbf{J}^* & \mathbf{D}^* \\ \mathbf{D}^{*T} & 0 \end{bmatrix}^{-1} = \begin{bmatrix} \mathbf{A} & \mathbf{B} \\ \mathbf{B}^T & \mathbf{C} \end{bmatrix} \tag{8}$$

From Eq. (6), it can be seen that

$$\dot{\Omega}^* = \mathbf{A}\mathbf{T}^*$$

From the equation

$$\begin{bmatrix} \mathbf{J}^* & \mathbf{D}^* \\ \mathbf{D}^{*T} & 0 \end{bmatrix} \cdot \begin{bmatrix} \mathbf{A} & \mathbf{B} \\ \mathbf{B}^T & \mathbf{C} \end{bmatrix} = \mathbf{I} \tag{9}$$

A, **B**, and **C** matrices are obtained from

$$\mathbf{B} = -\mathbf{J}^{*-T}\mathbf{D}^*\mathbf{C}^T \tag{10}$$

$$\mathbf{C}^T = -(\mathbf{D}^{*T}\mathbf{D}^*)^{-1}\mathbf{D}^{*T}\mathbf{J}^{*T}(\mathbf{D}^*\mathbf{D}^{*T})^{-1}\mathbf{D}^* \tag{11}$$

$$\mathbf{A} = \left[\mathbf{I} - \mathbf{J}^{*-T}\mathbf{D}^*(\mathbf{D}^{*T}\mathbf{J}^{*-1}\mathbf{D}^*)^{-T}\mathbf{D}^{*T}\right]\mathbf{J}^{*-1} \tag{12}$$

Because the size of A is $(3n-c)\times(3n-c)$, what we need is **A*** with the size of 6×6, where 6 represents the component number in this design.

Define another **Q** matrix with the size of $3n \times 6$

$$\mathbf{Q}_{3n\times 6} = \begin{bmatrix} \mathbf{I}_{6\times 6} \\ 0 \end{bmatrix} \tag{13}$$

Then, characteristics matrix **A*** can be written as below:

$$\mathbf{A}^{*\prime} = (\mathbf{NQ})^T\left\{\left[\mathbf{I} - \mathbf{J}^{*-T}\mathbf{D}^*(\mathbf{D}^{*T}\mathbf{J}^{*-1}\mathbf{D}^*)^{-T}\mathbf{D}^{*T}\right]\mathbf{J}^{*-1}\right\}(\mathbf{NQ}) \tag{14}$$

Thus, the matrix **A*** for all design candidates can be constructed automatically. Compared with the automated modeling in Refs. [11], [15], and [26], the proposed modeling method can be far more efficient and time-saving.

The problem, however, is that since the total number of designs is $60,480 \times C_{37}^3 = 4.7 \times 10^8$, the total design search space is very large.

In line with our design objective, several infeasibility conditions listed below are used to screen out a large number of infeasible designs.

Infeasible configurations:

(1) All three nodes of any PG have no connected component.
(2) Two outputs and the engine are connected to the same PG.
(3) If two configurations are identical except for two output shafts being swapped, then one of two configurations is deemed infeasible.
(4) If two configurations are identical except for two of the three motors being swapped, then one of the two configurations is deemed infeasible.

Following this step, the total number of feasible configurations reduces from 60,480 to 774.

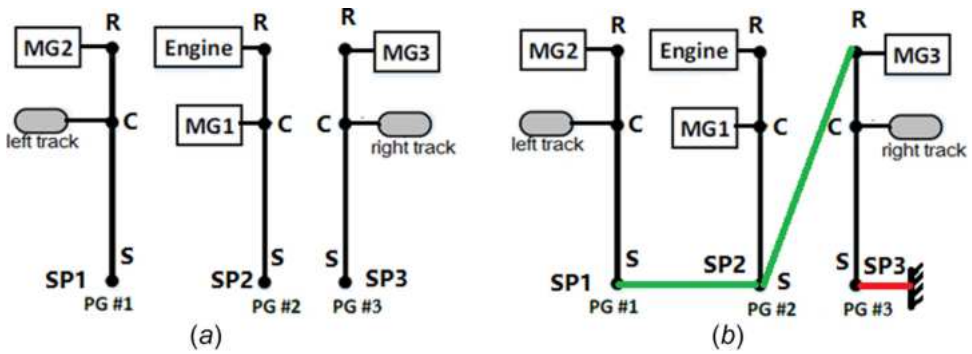

Fig. 5 An example of (*a*) a configuration and (*b*) a design

Table 2 Attribute screening conditions

Performance	Screening conditions
Two outputs controlled independently with engine on	$\text{rank}(A^*) = 3, \frac{a^*_{21}}{a^*_{22}} > 0, \frac{a^*_{31}}{a^*_{34}} > 0$
Steering while driving forward	$\text{rank}(A^*) = 3, \frac{a^*_{24}}{a^*_{22}} \cdot \frac{a^*_{34}}{a^*_{33}} < 0$ or $\frac{a^*_{25}}{a^*_{22}} \cdot \frac{a^*_{35}}{a^*_{33}} < 0$ or $\frac{a^*_{26}}{a^*_{22}} \cdot \frac{a^*_{36}}{a^*_{33}} < 0$
	$\frac{a^*_{21}}{a^*_{22}} < 0, \frac{a^*_{31}}{a^*_{33}} < 0$ or $\frac{a^*_{24}}{a^*_{22}} \cdot \frac{a^*_{34}}{a^*_{33}} > 0$
Driving backward	$or \frac{a^*_{25}}{a^*_{22}} \cdot \frac{a^*_{35}}{a^*_{33}} > 0$ or $\frac{a^*_{26}}{a^*_{22}} \cdot \frac{a^*_{36}}{a^*_{33}} > 0$

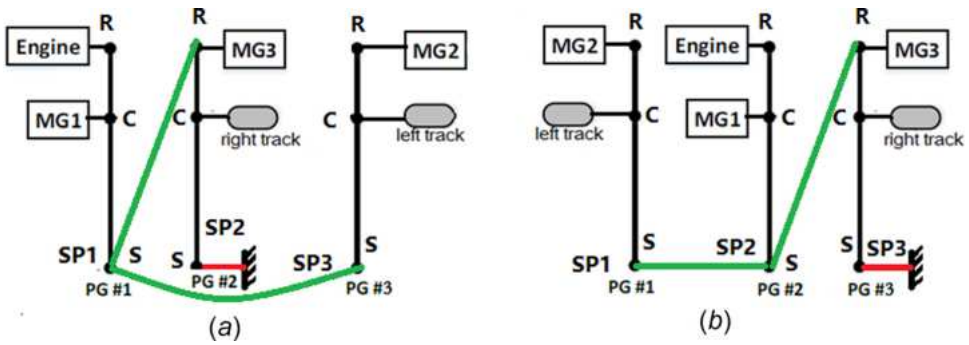

Fig. 6 An example of redundant designs

Infeasible permanent connections:

(1) Three connections from one node in a PG to all three nodes in another PG are not allowed.
(2) Three nodes in a PG are all grounded.
(3) Two nodes in one PG are connected, while the third is grounded.
(4) Two nodes of a PG are grounded, while any node of the same PG is used in another connection.
(5) The engine is grounded.
(6) Any node in a PG is free without any connection.

Following this step, the total number of feasible connections reduces from $C^3_{37} = 7770$ to 873. Thus, the total number of design candidates reduces to $873 \times 774 = 6.8 \times 10^5$. Using Eq. (10), the characteristic matrices of all designs are constructed for further screening.

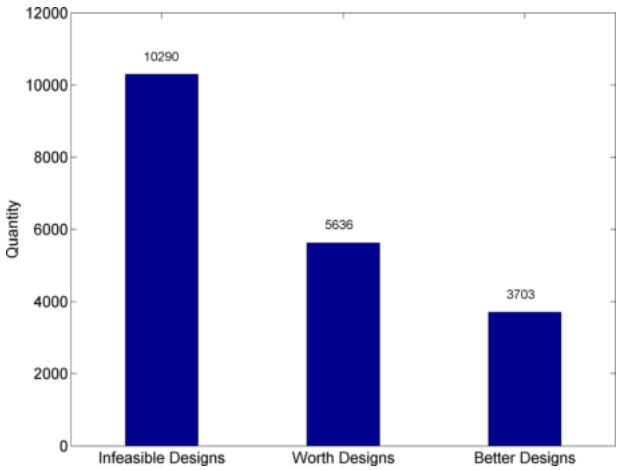

Fig. 7 Maximum torque screening results

4 Rapid Screening for Design Candidates

Although the design space is greatly reduced, the design space remains large. Thus, additional dynamic attribute screening is applied as follows.

4.1 Attribute Screening. For a TTD, several attributes are desired, namely, that the two output shafts can be controlled independently with the engine on, and the vehicle can be driven backward. These conditions are checked using the characteristics matrix. Define the elements of A^* in Eq. (15), the attribute screening conditions are listed in Table 2

$$A^* = \begin{bmatrix} a^*_{11} & a^*_{12} & a^*_{13} & a^*_{14} & a^*_{15} & a^*_{16} \\ a^*_{21} & a^*_{22} & a^*_{23} & a^*_{24} & a^*_{25} & a^*_{26} \\ a^*_{31} & a^*_{32} & a^*_{33} & a^*_{34} & a^*_{35} & a^*_{36} \\ a^*_{41} & a^*_{42} & a^*_{43} & a^*_{44} & a^*_{45} & a^*_{46} \\ a^*_{51} & a^*_{52} & a^*_{53} & a^*_{54} & a^*_{55} & a^*_{56} \\ a^*_{61} & a^*_{62} & a^*_{63} & a^*_{64} & a^*_{65} & a^*_{66} \end{bmatrix} \tag{15}$$

Since the rank of A^* equals to the degree-of-freedom [11], the rank of A^* should be 3. Write the second and third row of Eq. (7)

$$\begin{aligned} \frac{\dot{\omega}_{V\_l}}{a^*_{22}} &= \frac{a^*_{21}}{a^*_{22}} T_e + \frac{a^*_{23}}{a^*_{22}} T_{V\_r} + T_{V\_l} + \frac{a^*_{24}}{a^*_{22}} T_{\text{mg1}} + \frac{a^*_{25}}{a^*_{22}} T_{\text{mg2}} + \frac{a^*_{26}}{a^*_{22}} T_{\text{mg3}} \\ \frac{\dot{\omega}_{V\_r}}{a^*_{33}} &= \frac{a^*_{31}}{a^*_{33}} T_e + \frac{a^*_{32}}{a^*_{33}} T_{V\_l} + T_{V\_r} + \frac{a^*_{34}}{a^*_{33}} T_{\text{mg1}} + \frac{a^*_{35}}{a^*_{33}} T_{\text{mg2}} + \frac{a^*_{36}}{a^*_{33}} T_{\text{mg3}} \end{aligned} \tag{16}$$

From Eq. (16), if positive output torque at both output shafts can be controlled independently, then part of the driven torque must come from the engine, so we have $(a^*_{21}/a^*_{22}) > 0, (a^*_{31}/a^*_{34}) > 0$. Since the output torque for the two tracks may have opposite signs

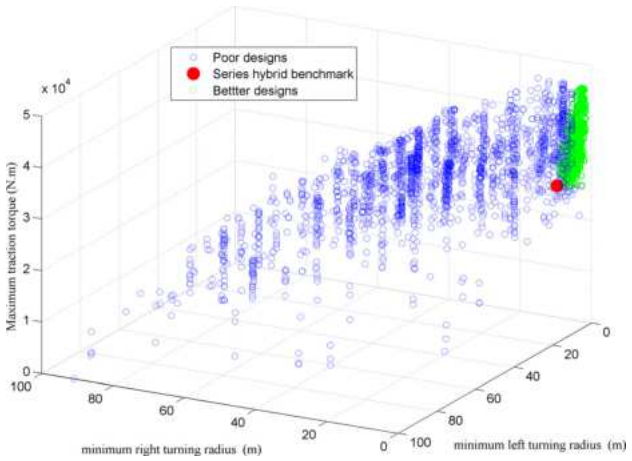

Fig. 8 Traction and turning performance screening

[30], the powertrain must realize turning both left and right by sending different torques to the two sides, with one of the motors providing the torque difference to achieve skid steering. For backward driving with engine-on, the engine torque should be in the opposite direction as the output torque. For driving backward with engine-off, the torque of one of the motors should have the opposite sign as the output torque.

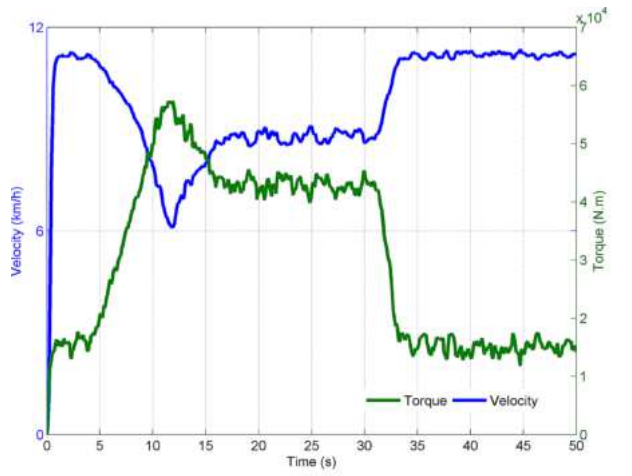

(*a*)

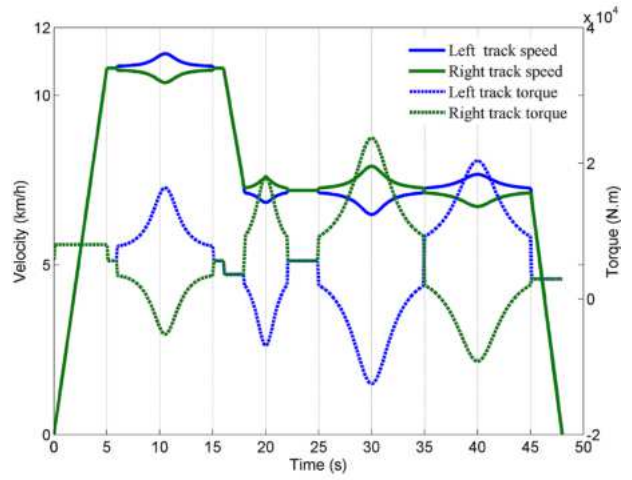

(*b*)

Fig. 9 Driving cycles: (*a*) straight driving and (*b*) turning

As a result of the attribute screening using A^* matrices, 109,363 designs survived from the 0.68 million designs. Among the surviving designs, some designs share the same A^* matrix. One of the examples is shown in Fig. 6, which swaps only the PG position. Only 19,619 designs were found to be unique among all 109,363 designs after uniqueness verification, which will pass on to the next design stage.

4.2 Performance Screening. In this design step, the driving performance of the designs is checked. The three motors are assumed to have the nominal size as shown in Table 1. All other parameters are the same as the series hybrid TTD. The engine and motors are both modeled as quasi-static models which are widely used in both industry and academia. Both the engine and motor characteristic maps are formed by the experimental data.

According to the ISO 53.100 standard for TTD, the towing capacity must be higher than a specific threshold at low operating speed. The maximum torques of all designs are shown in Fig. 7. Many of the designs cannot produce adequate torque at low speeds. Only 3703 designs survived the maximum torque screening in Fig. 7.

Next, the maximum traction torques and the minimum turning radius at all speeds for both left and right turns are calculated using Eqs. (1)–(4). To judge the overall performance, we have chosen the indices, the average of all speeds' maximum traction torque, and the average of all speeds' minimum turning radius, as in the below equation:

$$\bar{T} = \frac{\sum_{v=0}^{v_{\max}} T_{\max}(v)}{v_{\max}+1}; \quad \bar{R} = \frac{\sum_{v=1}^{v_{\max}} R_{\min}(v)}{v_{\max}} \tag{17}$$

where $T_{\max}(v)$ is the maximum traction torque for the design at the speed v. $R_{\min}(v)$ is the average minimum left and right turning radius for the design at the central speed v.

The x and y axes in Fig. 8 are the average of all speeds' minimum left and right turning radius, while the z axis is the average of all speeds' maximum traction torque. It can be seen from the figure that the red point is the performance of the series hybrid benchmark; the blue points represent worse designs, while the green points represent better designs. A total number of 97 designs have larger torque, smaller left and right turning radius compared with the benchmark according to Fig. 8.

4.3 Fuel Economy Screening. Unlike with wheeled vehicles, the driving cycle used to assess the overall fuel economy for TTDs should include small-radius turning. Since there is no typical cycle that integrates both straight driving and turning, two collected driving cycles are used to assess the straight driving and turning conditions separately.

The straight driving cycle is shown in Fig. 9(*a*) [27]. The blue line represents the speed, while the green one is the corresponding demand torque. The grade information is also included in the torque calculation. The cycle contains five stages: 1–4 s traveling; 4–16 s soil-cutting; 16–31 s soil-transportation; 31–33 s unloading; and 33–50 s no-load traveling.

The steering cycle is shown in Fig. 9(*b*) [31]. Since the speeds and torques of two tracks can be controlled independently, how steering is realized does not matter. More commonly used differential steering is adopted in the step. The solid line represents the speed and torque of the right track, while the dash line represents that of the left track. In 1–5 s, the TTD accelerates. And in 5–15 s, the TTD turns left with decreasing turning radius. In 15–17 s, the TTD decelerates and then turns right between 17 and 22 s. In 24–35 s, the TTD turns right again with decreasing radius. Then, it turns left again from 35 s to 45 s before stopping at 48 s.

The dynamic programming technique is used to implement optimal control under these cycles. The engine speed and state of charge (SOC) are the states, while the engine torque and the motor

toque are the control variables. By searching the engine speed and controlling the engine torque, the engine could be controlled to the sweet spot to ensure the overall efficiency. Using Eqs. (7)–(14), the automated dynamics modeling is used to calculate the speed and torque relationship in each DP step. DP could give the control executions of the engine and electric motor torque by splitting the mechanical and electrical power optimally. It should also be noted that the final SOC should equal the initial SOC in order to make a fair comparison of fuel consumption. Thus, the cost function combines two objectives: to minimize the fuel consumption and to keep SOC sustained

$$J = \sum_{k=0}^{N-1} L\big(x(k), u(k)\big) + \alpha(\mathrm{SOC}(N) - \mathrm{SOC}_{\mathrm{desired}})^2 \tag{18}$$

subject to :

$$\begin{cases} \begin{bmatrix} \dot{\omega}_e \\ \dot{\omega}_{V\_l} \\ \dot{\omega}_{V\_r} \\ \dot{\omega}_{\mathrm{mg1}} \\ \dot{\omega}_{\mathrm{mg2}} \\ \dot{\omega}_{\mathrm{mg3}} \end{bmatrix} = \mathrm{A}^* \begin{bmatrix} T_e \\ T_{V\_l} \\ T_{V\_r} \\ T_{\mathrm{mg1}} \\ T_{\mathrm{mg2}} \\ T_{\mathrm{mg3}} \end{bmatrix} \\ P_{\mathrm{Batt}} \le P_{\mathrm{Batt\_max}} \\ 0 \le T_e \le T_{e\_\mathrm{max}} \\ 0 \le \omega_e \le \omega_{e\_\mathrm{max}} \\ -T_{\mathrm{mg1\_max}}(\omega_{\mathrm{mg1}}) \le T_{\mathrm{mg1}} \le T_{\mathrm{mg1\_max}}(\omega_{\mathrm{mg1}}) \\ -\omega_{\mathrm{mg1\_max}} \le \omega_{\mathrm{mg1}} \le \omega_{\mathrm{mg1\_max}} \\ -T_{\mathrm{mg2\_max}}(\omega_{\mathrm{mg2}}) \le T_{\mathrm{mg2}} \le T_{\mathrm{mg2\_max}}(\omega_{\mathrm{mg2}}) \\ -\omega_{\mathrm{mg2\_max}} \le \omega_{\mathrm{mg2}} \le \omega_{\mathrm{mg2\_max}} \\ -T_{\mathrm{mg3\_max}}(\omega_{\mathrm{mg3}}) \le T_{\mathrm{mg3}} \le T_{\mathrm{mg3\_max}}(\omega_{\mathrm{mg3}}) \\ -\omega_{\mathrm{mg3\_max}} \le \omega_{\mathrm{mg3}} \le \omega_{\mathrm{mg3\_max}} \\ \mathrm{SOC}_{\mathrm{min}} \le \mathrm{SOC} \le \mathrm{SOC}_{\mathrm{max}} \end{cases} \tag{19}$$

where k is the time-step and 0 is the initial state, L represents the fuel consumption in each segment, N is the total number of steps, x and u are the state and control vector, respectively, and α is the weighing to keep SOC close to the desired value $\mathrm{SOC}_{\mathrm{desired}}$. The optimization must be subject to the engine, motor, and battery constraints.

The results of the 97 designs are shown in Fig. 10, where the x axis is the straight driving fuel economy and the y axis is the turning fuel economy. The red point is the fuel economy of the series hybrid benchmark. The actual-measured straight driving fuel economy in Ref. [27] is approximately 0.94 mpg, while the turning fuel economy is not considered. Thus, the paper employs the simulated results with the straight driving fuel economy 0.902 mpg and the turning fuel economy 0.759 mpg. The 15 designs shown in green circles are the superior designs that achieve better straight driving and turning fuel economy compared with the benchmark.

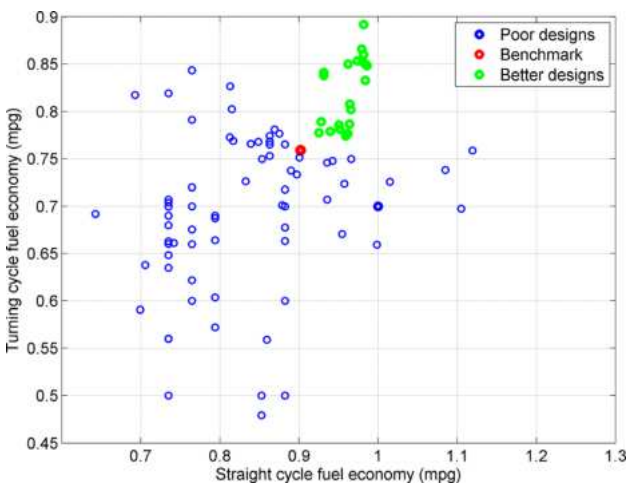

Fig. 10 Straight driving and turning fuel economy screening

The practicality analysis of the mechanical interference between PGs for manufacturing is not the focus in this paper. These 15 winning designs are summarized in Fig. 11. Parameter sizing of these designs are further explored in Sec. 5.

5 Enhanced Progressive Iteration of Topology Designs and Parameter Sizing

Up to now, the winning designs have all been based on arbitrarily selected design parameters. Topology optimization and sizing optimization are investigated together in this section.

Design parameters can be classified into two groups: one containing the gear ratio that includes the final drive of the right and left tracks and the gear ratio of the 3 PGs; the other containing the component sizes. Downsizing the power level of components can improve the efficiency and reduce the cost. The searched parameter values are listed below:

$$\begin{aligned} \mathrm{Fd}_l &= [64:4:76],\ \ \mathrm{Fd}_r = [64:4:76] \\ \mathrm{Gr}_1 &= [1.5:0.5:3],\ \ \mathrm{Gr}_2 = [1.5:0.5:3],\ \ \mathrm{Gr}_3 = [1.5:0.5:3] \\ \mathrm{Ps}_{\mathrm{eng}} &= [0.5:0.1:1] \\ \mathrm{Ps}_{\mathrm{battery}} &= [0.5:0.1:1] \\ \mathrm{Ps}_{\mathrm{mg1}} &= [0.5:0.1:1],\ \ \mathrm{Ps}_{\mathrm{mg1}} = [0.5:0.1:1],\ \ \mathrm{Ps}_{\mathrm{mg1}} = [0.5:0.1:1] \end{aligned} \tag{20}$$

The engine, motor, and battery sizes are represented by their scaling factors of the torque. The characteristic maps will change accordingly. Based on the 15 winning designs, there will be $15 \times 4^5 \times 6^5 = 1.13 \times 10^8$ designs with different parameters in Eq. (20).

The optimization problem can be formulated as in Eq. (21). The goal is to maximize the fuel economy and minimize the cost under the performance constraints. The former part in Eq. (21) represents the normalized fuel economy improvement while straight driving and steering. The latter part represents the normalized downsized power of all components, which can indicate the reduced cost. The fuel economy and the power size are normalized to ensure that two objectives are on the same value scale.

maximize

$$\begin{aligned} &\alpha_1 \left(\beta_1 \frac{L_{\mathrm{str}} - L_{\mathrm{des\_str}}}{L_{\mathrm{des\_str}}} + \beta_2 \frac{L_{\mathrm{ste}} - L_{\mathrm{des\_ste}}}{L_{\mathrm{des\_ste}}} \right) \\ &+\alpha_2 \left(\gamma_1 \frac{P_{\mathrm{eng\_des}} - P_{\mathrm{eng}}}{P_{\mathrm{eng\_des}}} + \gamma_2 \frac{P_{\mathrm{bat\_des}} - P_{\mathrm{bat}}}{P_{\mathrm{bat\_des}}} + \gamma_3 \frac{P_{\mathrm{mg\_des}} - P_{\mathrm{mg}}}{P_{\mathrm{mg\_des}}} \right) \end{aligned} \tag{21}$$

subject to

$$\begin{cases} T_{\mathrm{max}} \ge T_{\mathrm{max\_des}} \\ E_{\mathrm{max\_trq}} \ge E_{\mathrm{max\_trq\_des}} \\ E_{\mathrm{min\_radius}} \le E_{\mathrm{min\_radius\_des}} \\ L_{\mathrm{str}} \ge L_{\mathrm{des\_str}} \\ L_{\mathrm{ste}} \ge L_{\mathrm{des\_ste}} \end{cases} \tag{22}$$

where α_1 and α_2 are the weighing vectors of fuel economy and cost, respectively, β_1 and β_2 are the weighing vectors of straight and turning fuel economy, respectively, while γ_1, γ_2, and γ_3 are those of the cost of engine, battery, and motors, respectively. L_{str}

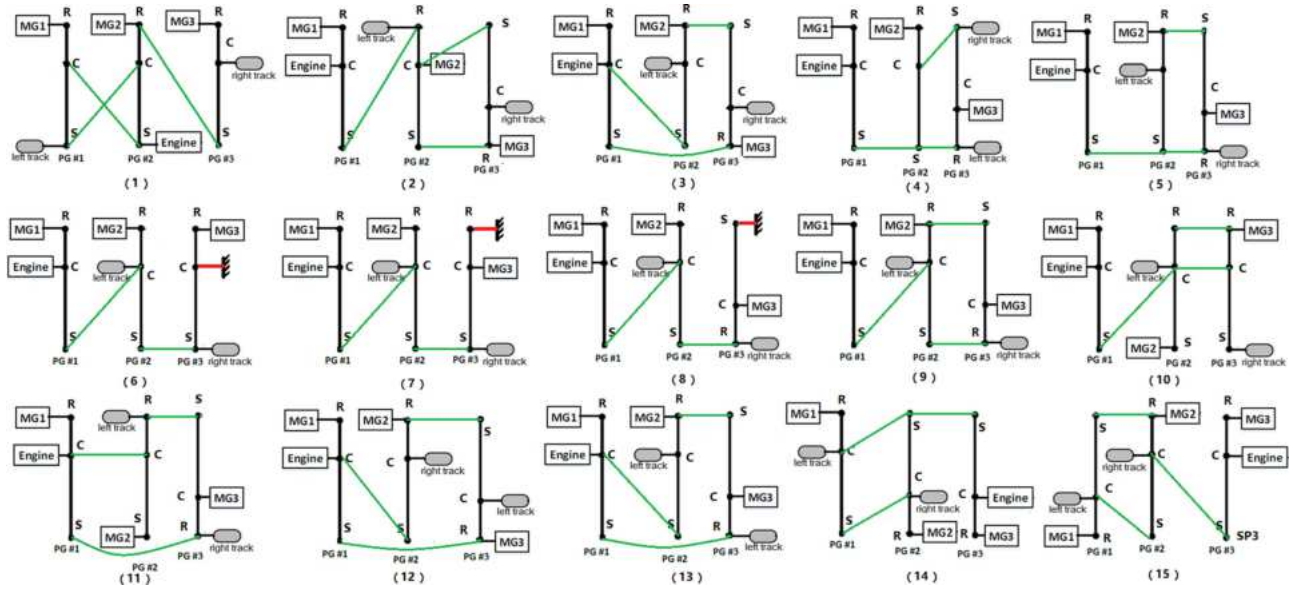

Fig. 11 Designs with superior fuel economy compared with the benchmark series hybrid

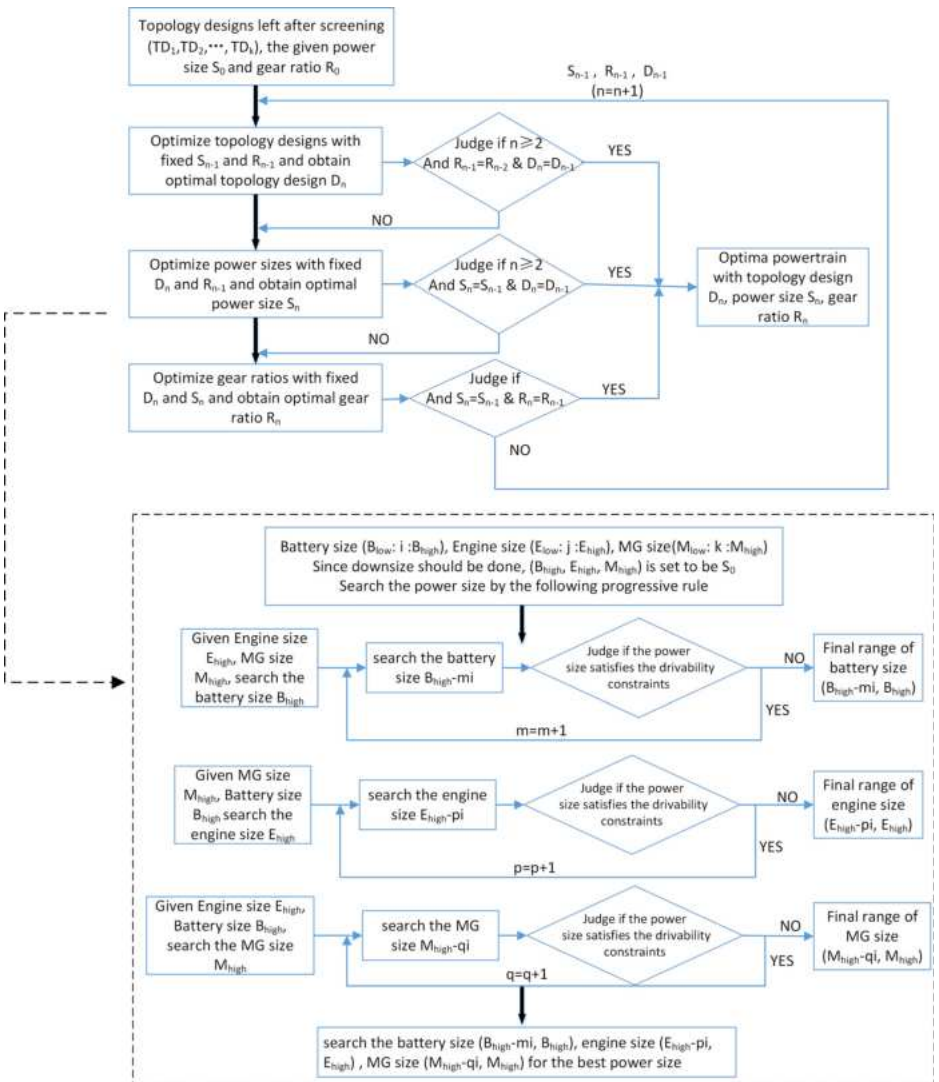

Fig. 12 The enhanced progressive iteration of topology designs and parameter sizing

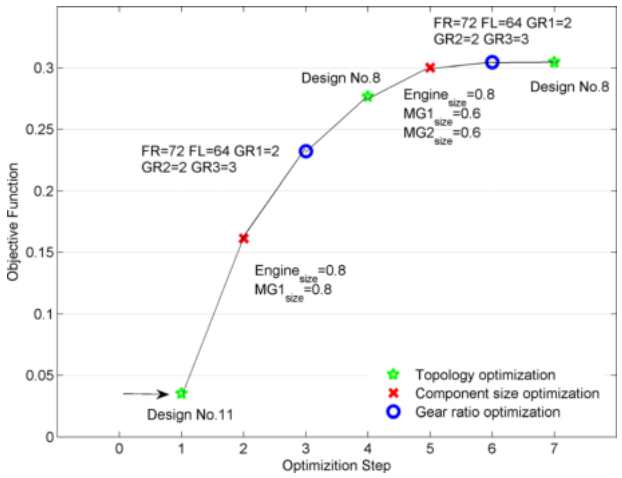

Fig. 13 Steps of topology design and parameter optimization

and L_{ste} represent the fuel economy of straight driving and turning, respectively. L_{des_str} and L_{des_ste} are the fuel economy of the series hybrid benchmark. P_{eng}, P_{bat}, and P_{mg} represent the downsized power of engine, battery, and motors, respectively, while P_{eng_des}, P_{bat_des}, and P_{mg_des} are the original sizes of components. T_{max} is the maximum towing torque of our design, while E_{max_trq} and E_{min_radius} are the expectations of maximum towing torque and minimum turning radius at all speeds, respectively.

We can see from Eq. (21) that the objective function has the physical meaning of the improvement compared with the benchmark. For example, when $\left(P_{eng\_des} - P_{eng}/P_{eng\_des}\right)$ is maximized, it means that the power size of P_{eng} is minimized. The objective is to downsize the components to reduce the power electronics cost.

The values of γ_1, γ_2, and γ_3 are determined by the component costs estimation method from Refs. [29] and [32]. In accordance with these references, γ_1 is set to be 0.3, γ_2 is set to be 0.1, and γ_3 is set to be 0.6. The values of α_1, α_2, β_1, and β_2, which can be flexible, are set to be 0.5 in this paper.

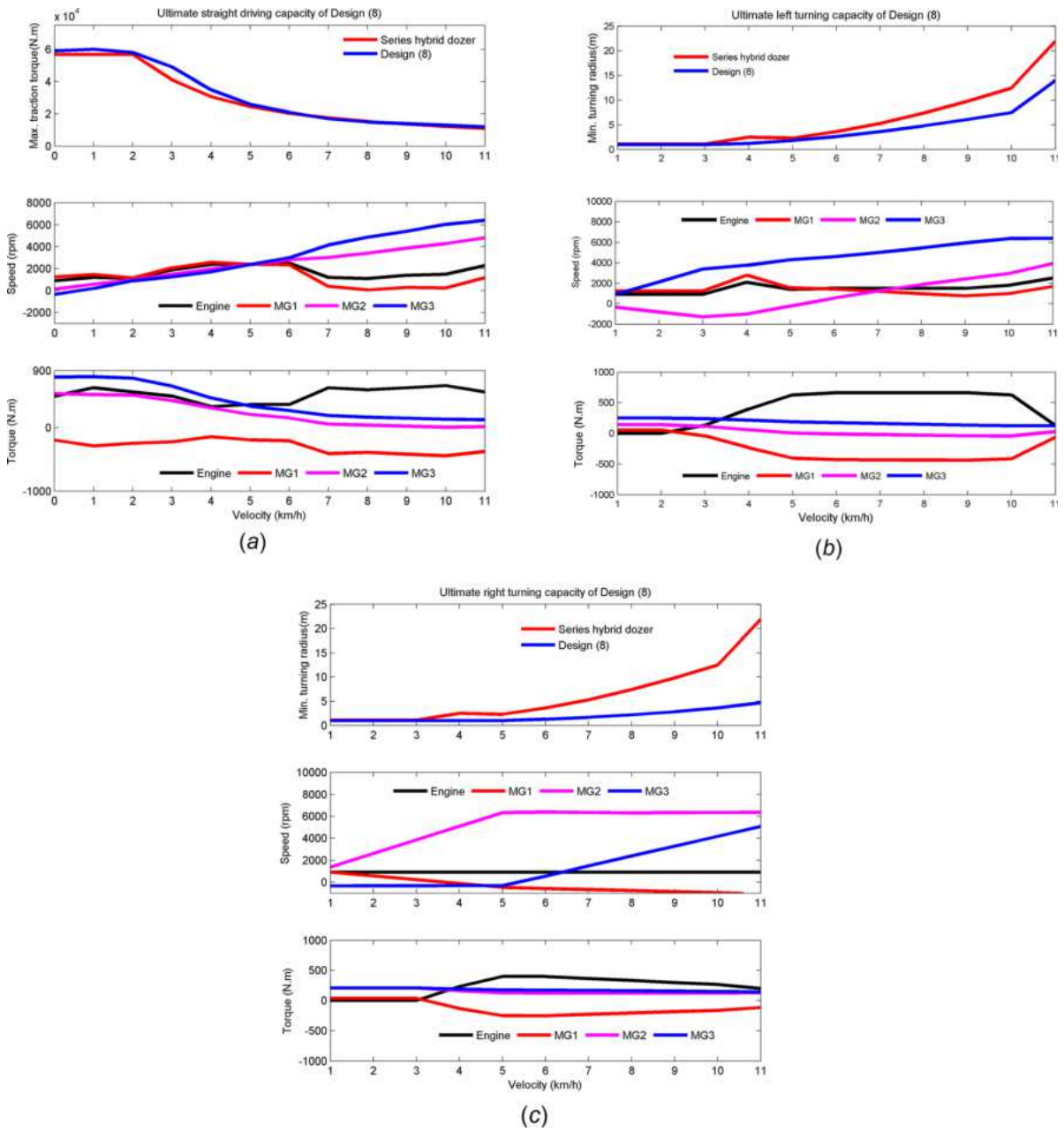

Fig. 14 Performance of the final optimal design: (*a*) straight driving, (*b*) left turning, and (*c*) right turning

The objective function in Eq. (21) is used to optimize the parameter sizes. Many parameter sizing methods can be used. The nested exhaustive search is too time-consuming and impractical. Genetic algorithms can also be used but the convergence is random and not guaranteed. The iterative optimization has been proved to converge to the global optimal results obtained from the nested optimization. The rate of convergence is much higher than the nested optimization and the global optima can be achieved after up to four iterations [33]. Based on the iterative optimization proposed in Ref. [26], an enhanced progressive iteration optimization approach is adopted. The concept is illustrated in Fig. 12.

As shown in Fig. 12, n, m, p, and q are the iteration numbers of each step. The iteration starts from the initial design D_0. Then, the loop begins in the first step that the topology is first optimized with the last iteration power size group S_{n-1} and gear ratio group R_{n-1} to obtain the optimized design D_n. In the second step, design D_n and gear ratio group R_{n-1} is fixed, while the power size group S_{n-1} is optimized (to S_n). Afterward, without changing topology D_n and power size group S_n, the gear ratio group is optimized to R_n. The loop must be checked at least once for the three types of variables, namely, designs, power size parameters, and gear ratio parameters. After the first loop, verification of the results in each step should be conducted. Iterations stop when the performance stops improving and the solution converges.

The power size and gear ratios are separated in the progressive iterations to reduce the computation load. The power size will not be exhaustively searched, as the search range is first checked using the constraints. For example, if the highest power size of engine E_{high} and motor M_{high} are fixed, the lowest power size of battery $B_{\text{high-mi}}$ that satisfies the constraints is calculated and

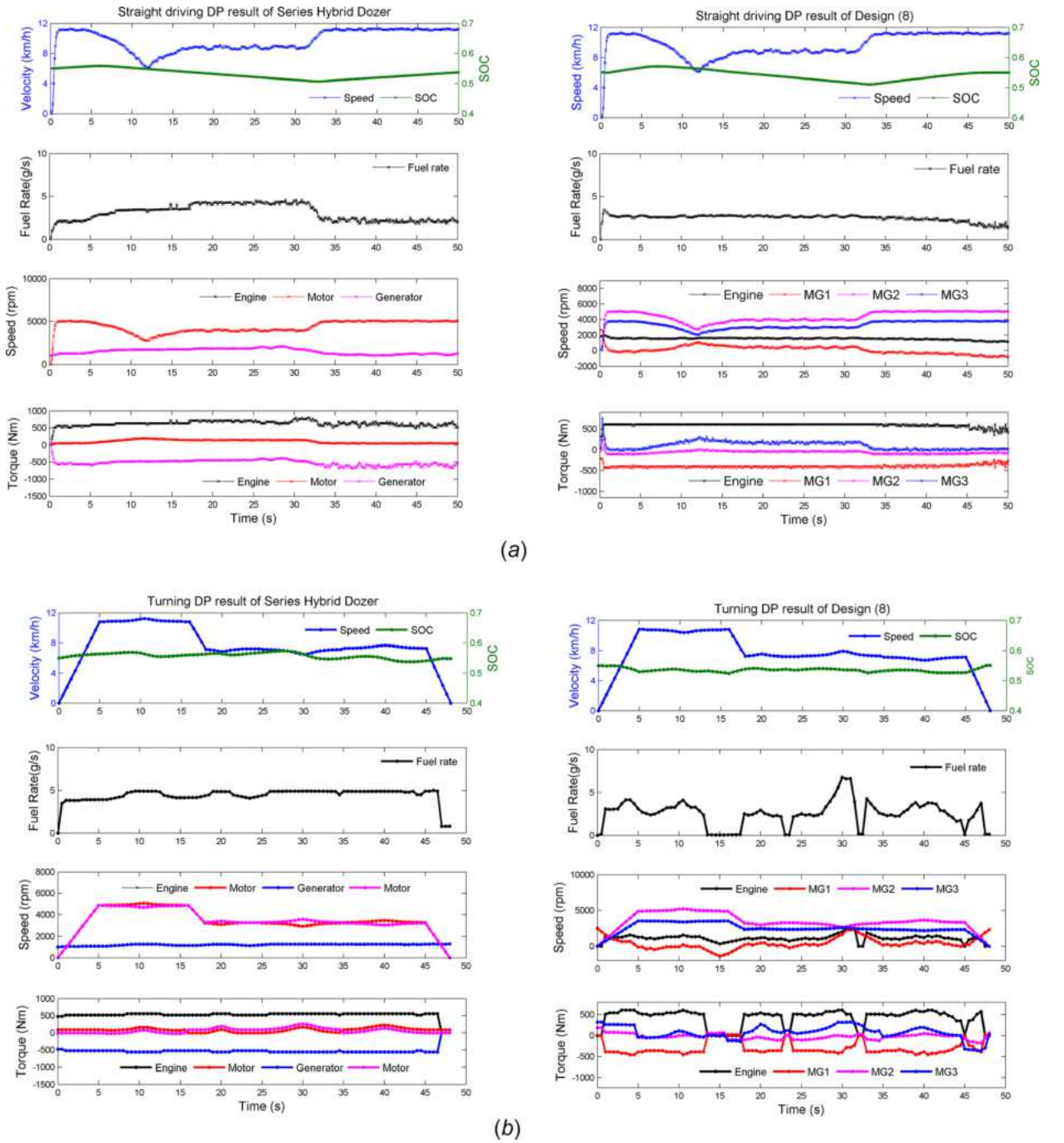

Fig. 15 (*a*) DP results while straight driving and (*b*) DP results while turning

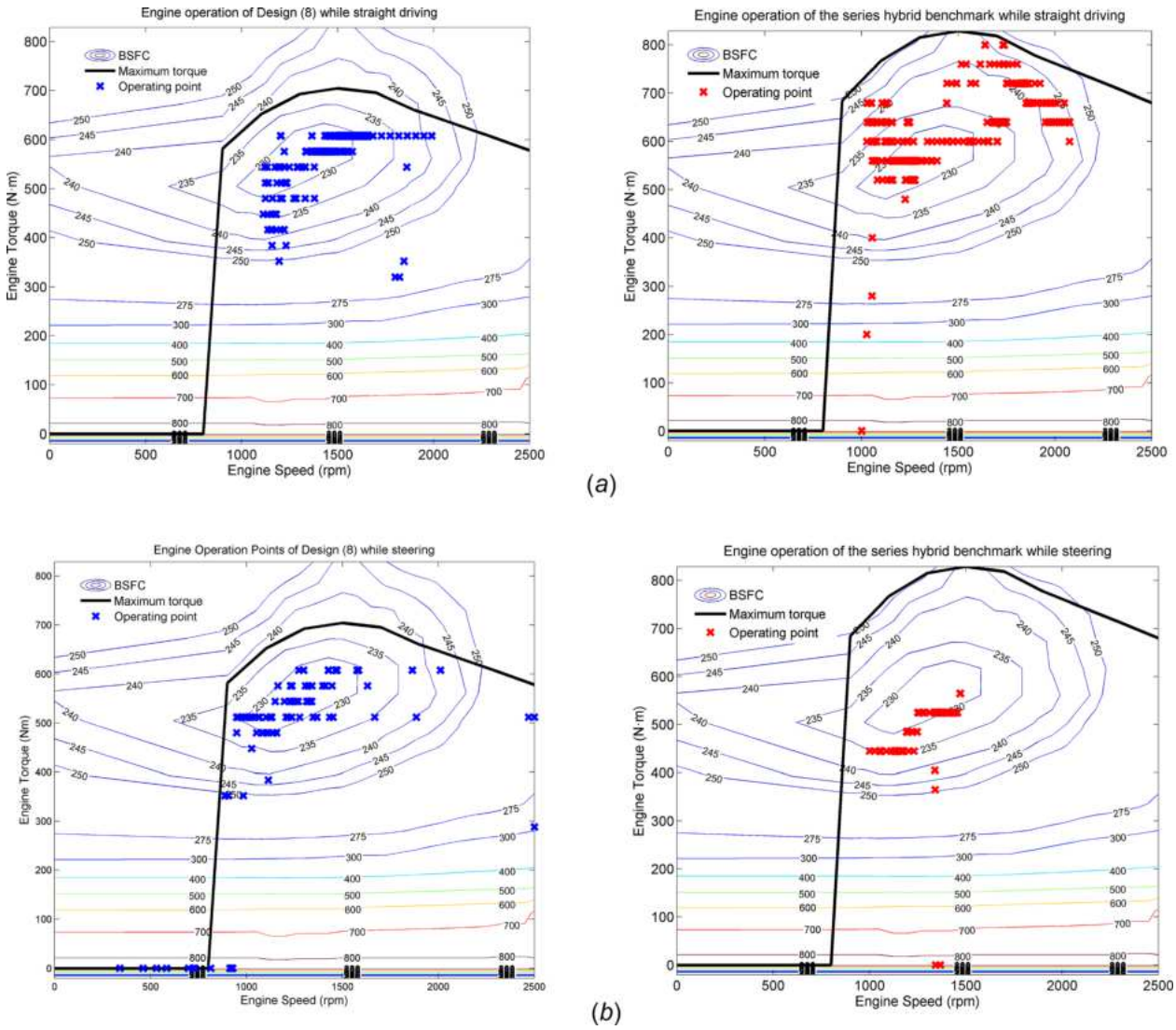

Fig. 16 (*a*) Engine operation points of design (8) and the benchmark during straight driving and (*b*) engine operation points of design (8) and the benchmark during turning

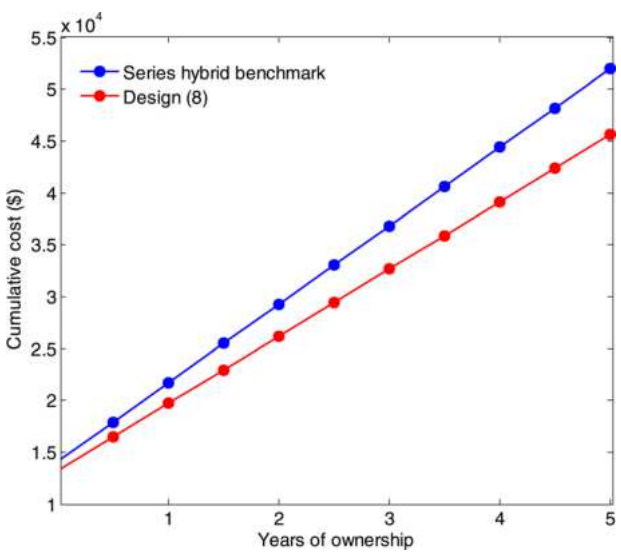

Fig. 17 Cumulative cost comparison

$B_{\text{high-mi}}$ will replace the given B_{low}. In other words, if the marginal value cannot satisfy the constraints, neither will the smaller one be able to.

The search results are presented in Fig. 13. FR and FL are the final drives of the right and left tracks, respectively. GR1, GR2, and GR3 are the gear ratio of the three PGs. After two loops, the topology design has converged to design No. 8 shown in Fig. 11, while the engine has been downsized to 80% and motors 1 and 2 have been downsized to 60% of the original.

The final drives on the two sides are 72 and 64, respectively. The gear ratios of the three PGs are 2.0, 2.0, and 3.0, respectively. To further show the advantages of our design, the overall performance is analyzed later.

The maximum straight driving torque of the optimal design compared with the benchmark at all speeds is shown in Fig. 14(*a*). The minimum turning radius compared with the benchmark at all speeds together with the operating states of the components is shown in Figs. 14(*b*) and 14(*c*), which represent left and right turning.

It can be seen that the performance of straight driving and turning of the optimal design is better than that of the series hybrid TTD. The final optimal design improves the average output torque

by 5.2% while straight driving, and improves the ability of left turning and right turning by 16% and 55%, respectively. Since the gradeability is related to the maximum traction torque, the detailed gradeability analysis is not included here.

The optimal control results of our design and benchmark are shown, respectively, in Fig. 15, which contain straight driving comparison together with the turning comparison.

The fuel economy of the series hybrid benchmark in Figs. 15(*a*) and 15(*b*) are 0.902 mpg and 0.759 mpg, while those of the right-sized design (8) are 1.032 mpg and 1.099 mpg. The fuel economy of the right-sized design (8) is 14.4% and 44.9% greater during straight driving and turning. The result confirms that using three motors indeed enlarges the design space and results in much better fuel economy compared with the series hybrid benchmark. The reason can be further explained by examining the engine operating points over the drive cycles in Fig. 16: the engine is always working near the sweet spot during both straight driving and turning.

For series hybrid benchmark, despite the fact that engine is also working near the sweet spot, the engine power has to be transferred two times to drive the vehicle. For our optimal design, part of the engine power can be transferred to the vehicle output directly, which improves the overall operating efficiency.

The power electronics cost of the final optimal design and the series hybrid benchmark is calculated [29,32]. To further explain the cumulative cost of our design and the series benchmark, the cost corresponding to years of ownership is shown in Fig. 17. Assuming that the TTD works 4 h per day and 150 days per year with the simulated straight driving fuel economy, the cumulative cost of both the design (8) and the series hybrid benchmark can be calculated. The power electronics of the series hybrid cost approximately 14,100 $, which is higher than the 13,230 $ of design (8). Furthermore, as time goes on, our design will become increasingly cost effective, which can be an important advantage for industrial application.

In summary, the power-split powertrain using three PGs with three motors greatly improves the fuel economy and also the drivability compared with the series hybrid benchmark. For future work, a multimode design with three motors can be researched to realize better integrated performance and downsize the battery for greater practicality.

6 Conclusion

In this paper, an efficient exhaustive search process for power-split hybrid powertrains with three PG is proposed. After screening and analyzing all the unique designs, superior fuel economy and dynamic performance designs are identified. The topologies of the powertrain, parameter sizes, and control are integrated together by developing an optimization framework. The main findings are summarized below:

(1) The power-split powertrain for TTD with three motors proposed can improve straight driving and turning performance by 5.2% and 35% approximately. The fuel economy is also improved by 14.4% and 44.9% during straight driving and turning, as the engine can be controlled to operate in the sweet spot to attain high efficiency.
(2) Not only straight driving but also turning proves the effectiveness of our design without any additional steering mechanism, thus showing great potential for TTD and other tracked vehicle designs.
(3) An enhanced progressive iteration optimization together with optimal control has been proposed to optimize the topology designs, parameters such as gear ratios, and power sizes of components evolutionary, which can quickly converge to an optimal design when there are many variables.
(4) The proposed novel propulsion system and the novel design methodology can also be applied to power-split wheeled vehicles to identify the optimal design rapidly.

Funding Data

- The National Key R&D Program of China (Grant No. 2016YFB0100905).
- The National Natural Science Foundation of China (Grant No. 51575295).

References

[1] Yaegashi, T., Sasaki, S., and Abe, T., 1998, "Toyota Hybrid System: It's Concept and Technologies," World Automobile Congress (FISITA98), Paris, France, Paper No. F98TP095.
[2] Duoba, M., Ng, H., and Larsen, R., 2001, "Characterization and Comparison of Two Hybrid Electric Vehicles (HEVs)-Honda Insight and Toyota Prius," SAE Paper No. 2001-01-1335.
[3] Grewe, T. M., Conlon, B. M., and Holmes, A. G., 2007, "Defining the General Motors 2-Mode Hybrid Transmission," SAE Paper No. 2007-01-0273.
[4] Cobb, J., 2016, "December 2016 Dashboard," HybridCars, Toronto, ON, Canada, accessed Jan 5, 2017, http://www.hybridcars.com/december-2016-dashboard/
[5] Mantriota, G., 2001, "Theoretical and Experimental Study of a Power Split Continuously Variable Transmission System—Part 1," Proc. Inst. Mech. Eng., Part D, **215**(7), pp. 837–850.
[6] Benford, H., and Leising, M., 1981, "The Lever Analogy: A New Tool in Transmission Analysis," SAE Paper No. 810102.
[7] Liu, J., 2007, "Modeling, Configuration and Control Optimization of Power-Split Hybrid Vehicles," Ph.D. thesis, The University of Michigan, Ann Arbor, MI.
[8] Conlon, B., 2005, "Comparative Analysis of Single and Combined Hybrid Electrically Variable Transmission Operating Modes," SAE Paper No. 2005-01-1162.
[9] Yang, H., Kim, B., Park, Y., Lim, W., and Cha, S., 2009, "Analysis of Planetary Gear Hybrid Powertrain System—Part 2: Output Split System," Int. J. Autom. Technol., **10**(3), pp. 381–390.
[10] Holmes, A. G., Schmidt, M. R., and Klemen, D., 2003, "Three-Mode, Compound-Split, Electrically-Variable Transmission," Motors Liquidation Company, Detroit, MI, U.S. Patent No. 6,551,208.
[11] Zhang, X., Li, S. E., Peng, H., and Sun, J., 2015, "Efficient Exhaustive Search of Power-Split Hybrid Powertrains With Multiple Planetary Gears and Clutches," ASME J. Dyn. Syst., Meas., Control, **137**(12), p. 121006.
[12] Bayrak, A. E., Ren, Y., and Papalambros, P. Y., 2013, "Design of Hybrid-Electric Vehicle Architectures Using Auto-Generation of Feasible Driving Modes," ASME Paper No. DETC2013-13043.
[13] Silvas, E., Hofman, T., Serebrenik, A., and Steinbuch, M., 2015, "Functional and Cost-Based Automatic Generator for Hybrid Vehicles Topologies," IEEE/ASME Trans. Mechatronics, **20**(4), pp. 1561–1572.
[14] Li, C. T., and Peng, H., 2010, "Optimal Configuration Design for Hydraulic Split Hybrid Vehicles," American Control Conference (ACC), Baltimore, MD, June 30–July 2, pp. 5812–5817.
[15] Pan, Z., Zhang, X., Silvas, E., Peng, H., and Ravi, N., 2015, "Optimal Design of All-Wheel-Drive Hybrid Pick-Up Trucks," ASME Paper No. DSCC2015-9701.
[16] Galvagno, E., Rondinelli, E., and Velardocchia, M., 2012, "Electro-Mechanical Transmission Modelling for Series-Hybrid Tracked Tanks," Int. J. Heavy Veh. Syst., **19**(3), pp. 256–280.
[17] Zou, Y., Sun, F., Hu, X., Guzzella, L., and Peng, H., 2012, "Combined Optimal Sizing and Control for a Hybrid Tracked Vehicle," Energies, **5**(11), pp. 4697–4710.
[18] Shabana, A. A., 1997, *Nonlinear Dynamics of Tracked Vehicles*, Chicago University, Hyde Park, IL.
[19] Chen, Z. Y., and Zhao, G. Y., 2012, "Fuzzy Control Strategy and Simulation for Dual Electric Tracked Vehicle Motion Control," Appl. Mech. Mater., **130–134**, pp. 309–312.
[20] Schmidt, M. R., 2002, "Two-Mode, Compound-Split, Electro-Mechanical, Vehicular Transmission Particulary Adapted for Track-Laying Vehicles," Motors Liquidation Company, Detroit, MI, U.S. Patent No. 6,491,599.
[21] Silvas, E., Hofman, T., Murgovski, N., Etman, L. P., and Steinbuch, M., 2017, "Review of Optimization Strategies for System-Level Design in Hybrid Electric Vehicles," IEEE Trans. Veh. Technol., **66**(1), pp. 57–70.
[22] Galdi, V., Ippolito, L., Piccolo, A., and Vaccaro, A., 2001, "A Genetic-Based Methodology for Hybrid Electric Vehicles Sizing," Soft Comput., **5**(6), pp. 451–457.
[23] Zhang, B., Chen, Z., Mi, C., and Murphey, Y. L., 2009, "Multi-Objective Parameter Optimization of a Series Hybrid Electric Vehicle Using Evolutionary Algorithms," Vehicle Power and Propulsion Conference (VPPC'09), Dearborn, MI, Sept. 7–10, pp. 921–925.
[24] Long, V. T., and Nhan, N. V., 2012, "Bees-Algorithm-Based Optimization of Component Size and Control Strategy Parameters for Parallel Hybrid Electric Vehicles," Int. J. Autom. Technol., **13**(7), pp. 1177–1183.
[25] Wu, J., Zhang, C. H., and Cui, N. X., 2008, "PSO Algorithm-Based Parameter Optimization for HEV Powertrain and Its Control Strategy," Int. J. Autom. Technol., **9**(1), pp. 53–59.
[26] Zhuang, W., Zhang, X., Peng, H., and Wang, L., 2016, "Rapid Configuration Design of Multiple-Planetary-Gear Power-Split Hybrid Powertrain Via Mode Combination," IEEE/ASME Trans. Mech., **21**(6), pp. 2924–2934.

[27] Zou, Y., Chen, X., and Li, D., 2014, "Parameter Matching Design and Control Optimization for Series Hybrid Tracked Bulldozer," ASME J. Mech. Eng., **50**(1), pp. 70–75.
[28] Zhuang, W., Zhang, X., Ding, Y., and Wang, L., 2016, "Comparison of Multi-Mode Hybrid Powertrains With Multiple Planetary Gears," Appl. Energy, **178**, pp. 624–632.
[29] Golbuff, S., 2006, "Optimization of a Plug-In Hybrid Electric Vehicle," M.S. thesis, Georgia Institute of Technology, Atlanta, Georgia.
[30] Shanmuganathan, U., Govarthanan, R., Muthumailvaganan, A., and Imayakumar, A., 2006, "Modeling and Dynamic Simulation of IC Engine Driven Permanent Magnet Generator Using Matlab/Simulink for Hybrid Tracked Vehicle," Conference on Electric and Hybrid Vehicles (ICEHV), Pune, India, Dec. 18–20, pp. 1–6.
[31] Zhang, B., Zhang, X., and Xi, L., 2015, "Modelling and Economy Performance Simulation of Hybrid Electric Bulldozer Under Whole Operation Cycles," Trans. Chin. Soc. Agric. Mach., **46**(6), pp. 294–302.
[32] Graham, R., 2001, "Comparing the Benefits and Impacts of Hybrid Electric Vehicle Options," Electric Power Research Institute (EPRI), Palo Alto, CA, Report No. 1006892.
[33] Kelley, C. T., 1999, *Iterative Methods for Optimization*, Society for Industrial and Applied Mathematics, Philadelphia, PA.